



Ab initio calculation of lattice dynamics and thermodynamic properties of beryllium

Fen Luo, Ling-Cang Cai, Xiang-Rong Chen, Fu-Qian Jing, and Dario Alfè

Citation: *J. Appl. Phys.* **111**, 053503 (2012); doi: 10.1063/1.3688344

View online: <http://dx.doi.org/10.1063/1.3688344>

View Table of Contents: <http://jap.aip.org/resource/1/JAPIAU/v111/i5>

Published by the [American Institute of Physics](http://www.aip.org).

Related Articles

Metal induced crystallization mechanism of the metal catalyzed growth of silicon wire-like crystals
Appl. Phys. Lett. **99**, 143102 (2011)

Note: Extraction of hydrogen bond thermodynamic properties of water from dielectric constant and relaxation time data

J. Chem. Phys. **135**, 086101 (2011)

Waste-recycling Monte Carlo with optimal estimates: Application to free energy calculations in alloys

J. Chem. Phys. **135**, 044127 (2011)

Particle-based multiscale coarse graining with density-dependent potentials: Application to molecular crystals (hexahydro-1,3,5-trinitro-s-triazine)

J. Chem. Phys. **135**, 044112 (2011)

Stacking in sediments of colloidal hard spheres

J. Chem. Phys. **135**, 034510 (2011)

Additional information on J. Appl. Phys.

Journal Homepage: <http://jap.aip.org/>

Journal Information: http://jap.aip.org/about/about_the_journal

Top downloads: http://jap.aip.org/features/most_downloaded

Information for Authors: <http://jap.aip.org/authors>

ADVERTISEMENT

	Working @ low temperatures? Contact Janis for Cryogenic Research Equipment Click here to browse our site at www.janis.com	
---	---	---

Ab initio calculation of lattice dynamics and thermodynamic properties of beryllium

Fen Luo,^{1,2} Ling-Cang Cai,^{1,a)} Xiang-Rong Chen,^{2,3,b)} Fu-Qian Jing,^{1,2} and Dario Alfè⁴

¹National Key Laboratory for Shock Wave and Detonation Physics Research, Institute of Fluid Physics, Chinese Academy of Engineering Physics, Mianyang 621900, China

²College of Physical Science and Technology, Sichuan University, Chengdu 610064, China

³International Centre for Materials Physics, Chinese Academy of Sciences, Shenyang 110016, China

⁴Department of Earth Sciences, University College London, Gower Street, London WC1E 6BT, United Kingdom

(Received 17 October 2011; accepted 18 January 2012; published online 1 March 2012)

We investigate the phase transition, elastic constants, phonon dispersion curves, and thermal properties of beryllium (Be) at high pressures and high temperatures using density functional theory. By comparing the Gibbs free energy, in the quasiharmonic approximation (QHA), of hexagonal-closed-packed (hcp) with those of the face-centered cubic (fcc) and body-centered-cubic (bcc) we find that the hcp Be is stable up to 390 GPa, and then transforms to the bcc Be. The calculated phonon dispersion curves are in excellent agreement with experiments. Under compression, the phonon dispersion curves of hcp Be do not show any anomaly or instability. At low pressure the phonon dispersion of bcc Be display imaginary along Γ -N in the T_1 branches. Within the quasiharmonic approximation, we predict the thermal equation of state and other properties including the thermal expansion coefficient, Hugoniot curves, heat capacity, Grüneisen parameter, and Debye temperature. © 2012 American Institute of Physics. [<http://dx.doi.org/10.1063/1.3688344>]

I. INTRODUCTION

Beryllium has a wide range of applications in aircrafts, spacecrafts, communication satellites, nuclear power industry and so on.¹ In addition, Be can also be alloyed with other elements to produce strong lightweight alloys for computer parts and instruments, and other applications.² For those important applications, scientific investigations on structural stability and phase diagram of beryllium have attracted tremendous experimental and theoretical interest.^{3–14}

At ambient condition, Be has the hexagonal-closed-packed (hcp) structure and melts at 1560 K.³ It transforms to the body-centered-cubic (bcc) structure at 1523 K.⁴ Experimentally, Ming *et al.*⁵ found the existence of a distorted hcp phase at pressures between 8.6 and 14.5 GPa. Nakano *et al.*⁶ investigated the static compression of Be by x-ray diffraction and found that the hcp phase was stable up to 171 GPa at 300 K. The hcp Be was found to be stable to the highest pressure of 66 GPa by Velisavljevic *et al.*⁷ Evans *et al.*⁸ confirmed the stability of hcp Be to 200 GPa at 300 K with x-ray and Raman studies in helium and argon pressure media. Theoretically, Lam *et al.*⁹ predicted that the stable phase is either bcc or face-centered-cubic (fcc) between 100 and 200 GPa using the pseudopotential method. Meyer-ter-Vehn *et al.*¹⁰ showed that hcp Be transformed directly to bcc Be at 200 GPa based on the augmented spherical waves method. Later, Palanivel *et al.*¹¹ obtained that the lowest energy phase is bcc Be above 180 GPa, using the full-potential linear muffin-tin orbital (FP-LMTO) method. Sin'ko *et al.*¹² used the FP-LMTO method and discovered that hcp-bcc phase transition

pressure is 270 GPa at 300 K. Moreover, the phase boundaries of the hcp-bcc phase transition were calculated by Benedict *et al.*¹³ and Robert *et al.*,¹⁴ and they all predicted the hcp phase as the most stable structure up to 400 GPa at 0 K. Although Be has a simple atomic structure, it remains challenging to accurately determine its phase transitions.

It is important to have a systematic study of the thermal equation of state (EOS) to understand the phase diagram and dynamical response of materials under extreme conditions. The elastic properties of materials at high pressure are important because they relate to various fundamental physical properties such as mechanical strength, and the EOS. The elastic constants have been measured at ambient condition¹⁵ or high temperature.^{16,17} Based on density-functional theory, the elastic constants of Be have been investigated by several groups.^{2,12,18} However, the investigations of thermal EOS and elastic properties of Be under extreme conditions are still scarce. In the present work, we focus on the thermodynamic and elastic properties of Be under high pressure.

In a neutron scattering experiment,¹⁹ the low-temperature phonon dispersion relation of the hcp phase of Be did not show any anomaly or instability at ambient pressure. Theoretically, combining frozen phonon and density-functional perturbation theory methods, Robert *et al.*^{20,21} obtained the phonon dispersion relations of hcp Be and bcc Be at different densities. They have been successful at reproducing the experimental investigation and found that the hcp phase is stable from 1.4 to 6 g/cc. At ambient conditions, the phonon dispersion relation of bcc Be exhibited a large softening near the N point of the T_1 branch along the Γ -N direction, which showed that the bcc phase is unstable. The frequency near 2/3 [111] transverse mode is also anomalous low when the density decreases under 1.65 g/cc. One of the main purposes of this

^{a)}Electronic mail: cai_lingcang@yahoo.com.cn.

^{b)}Electronic mail: xrchen@126.com.

work is to investigate the lattice dynamics and thermodynamics of Be under high pressure and temperature.

Here, we apply density functional perturbation theory (DFPT)^{22,23} to investigate a wide range of properties, including the lattice dynamical properties, the thermal EOS and thermodynamic properties of Be under high pressure. First, we discuss the structural and elastic properties of Be under high pressure. Then, we study the phase diagram and the thermodynamic properties within the quasiharmonic approximation (QHA).

II. COMPUTATIONAL METHOD

According to QHA, the free energy is given by

$$F(V, T) = E_{static}(V) + F_{phon}(V, T) + F_{elec}(V, T), \quad (1)$$

where $E_{static}(V)$ is the energy of a static lattice at zero temperature T and volume V , $F_{elec}(V, T)$ is the thermal free energy arising from electronic excitations, and $F_{phon}(V, T)$ is the phonon contribution. Both $E_{static}(V)$ and $F_{elec}(V, T)$ can be evaluated via static first-principles calculations directly. The phonon vibrational contribution $F_{phon}(V, T)$ can be expressed as

$$F_{phon}(V, T) = \frac{1}{2} \sum_{q,j} \hbar \omega_j(q, V) + k_B T \sum_{q,j} \ln \{ 1 - \exp[-\hbar \omega_j(q, V)/k_B T] \}, \quad (2)$$

where k_B is the Boltzmann constant, \hbar is the Planck constant divided by 2π , and $\omega_j(q, V)$ is the phonon frequency of the j th mode of wave vector q in the first Brillouin zone (BZ). The phonon dispersion calculations of Be have been performed within DFPT as implemented in the QUANTUM ESPRESSO package²⁴ using local-density approximation (LDA)²⁵ with the parametrization of Perdew and Zunger.²⁶ A nonlinear core correction to the exchange-correlation energy function was introduced to generate a norm-conserving pseudopotential²⁷ for Be with the valence electrons configuration $2s^2$. The pseudopotential was generated with a nonrelativistic calculation using the LDA.

To ensure the convergence of phonon frequencies and free energies, we made careful tests on k and q grids, the kinetic energy cutoff, and smearing parameters. For hcp Be, dynamical matrices were computed at 28 wave (q) vectors using an $6 \times 6 \times 6$ q grid in the irreducible wedge of the Brillouin zone. The plane wave cutoff for the wave functions was 60 Ry. The Monkhorst-Pack (MP)²⁸ meshes were $20 \times 20 \times 14$ for hcp Be and $20 \times 20 \times 20$ for bcc Be in both total energy and phonon dispersion calculations, respectively. We computed the dynamical matrices at 29 wave (q) vectors using the $8 \times 8 \times 8$ q grid for bcc Be in the irreducible wedge of the BZ, and the full phonon dispersion was obtained through Fourier interpolation. We applied a Fermi-Dirac smearing width of 0.02 Ry. The geometric mean phonon frequency is defined by

$$\ln \bar{\omega} = \frac{1}{N_{qj}} \sum_{qj} \ln \bar{\omega}_{qj}, \quad (3)$$

where ω_{qj} is the phonon frequency of the branch j at the wave vector q and N_{qj} is the number of branches times the total number of q points in the sum. With this choice of parameters, the geometric mean phonon frequency $\bar{\omega}$ was converged to 1 cm^{-1} .

The elastic constants are defined by means of a Taylor expansion of the total energy, $E(V, \delta)$, for the system with respect to a small strain δ of the lattice primitive cell volume V . The energy of a strained system is expressed as follow

$$E(V, \delta) = E(V_0, 0) + V_0 \left[\sum_i \tau_i \zeta_i \delta_i + \frac{1}{2} \sum_{ij} C_{ij} \delta_i \zeta_j \delta_j \right], \quad (4)$$

where $E(V_0, 0)$ is the energy of the unstrained system with equilibrium volume V_0 , τ_i is an element in the stress tensor, and ζ_i is a factor to take care of the Voigt index.²⁹

The elastic constants of Mo³⁰ and Ti³¹ were successfully obtained using the theoretical method proposed by Sin'ko and Smirnov.³² Here we give a description of this method. The lattice vectors \mathbf{a}' of the strained primitive cell are determined from the lattice vectors \mathbf{a} of the equilibrium primitive cell by the relation $\mathbf{a}' = \mathbf{a}(I + \hat{\varepsilon}_i)$, where I is the unit matrix and $\hat{\varepsilon}_i$ is a strain tensors. To calculate five independent constants of hexagonal structures, we considered five independent volume-nonconserving strains

$$\begin{aligned} \hat{\varepsilon}_1 &= \begin{pmatrix} \gamma & 0 & 0 \\ 0 & 0 & 0 \\ 0 & 0 & \gamma \end{pmatrix}, & \hat{\varepsilon}_2 &= \begin{pmatrix} \gamma & 0 & 0 \\ 0 & -\gamma & 0 \\ 0 & 0 & 0 \end{pmatrix}, \\ \hat{\varepsilon}_3 &= \begin{pmatrix} \gamma & 0 & 0 \\ 0 & \gamma & 0 \\ 0 & 0 & 0 \end{pmatrix}, & \hat{\varepsilon}_4 &= \begin{pmatrix} 0 & 0 & \gamma \\ 0 & 0 & 0 \\ \gamma & 0 & 0 \end{pmatrix}, & \hat{\varepsilon}_5 &= \begin{pmatrix} 0 & 0 & 0 \\ 0 & 0 & 0 \\ 0 & 0 & \gamma \end{pmatrix}. \end{aligned} \quad (5)$$

The specific energy of the crystal deformed in accord with the $\hat{\varepsilon}_1$ was calculated as a function of the strain magnitude γ . The values of strain γ with the range of $\pm 5\%$ were used to make the strain energy fit to a second-order polynomial function. Then the strain energy as a function of the strain can be written as

$$C_{11} + 2C_{13} + C_{33} - 2P = \rho_1 \left. \frac{d^2 E(\rho_1, \hat{\varepsilon}_1)}{d\gamma^2} \right|_{\gamma=0}, \quad (6)$$

where P was the pressure applied. Similar results with the other matrix were used in the equation

$$2(C_{11} - C_{12} - P) = \rho_1 \left. \frac{d^2 E(\rho_1, \hat{\varepsilon}_2)}{d\gamma^2} \right|_{\gamma=0}, \quad (7)$$

$$2(C_{11} + C_{12} - P) = \rho_1 \left. \frac{d^2 E(\rho_1, \hat{\varepsilon}_3)}{d\gamma^2} \right|_{\gamma=0}, \quad (8)$$

$$4C_{44} - 2P = \rho_1 \left. \frac{d^2 E(\rho_1, \hat{\varepsilon}_4)}{d\gamma^2} \right|_{\gamma=0}, \quad (9)$$

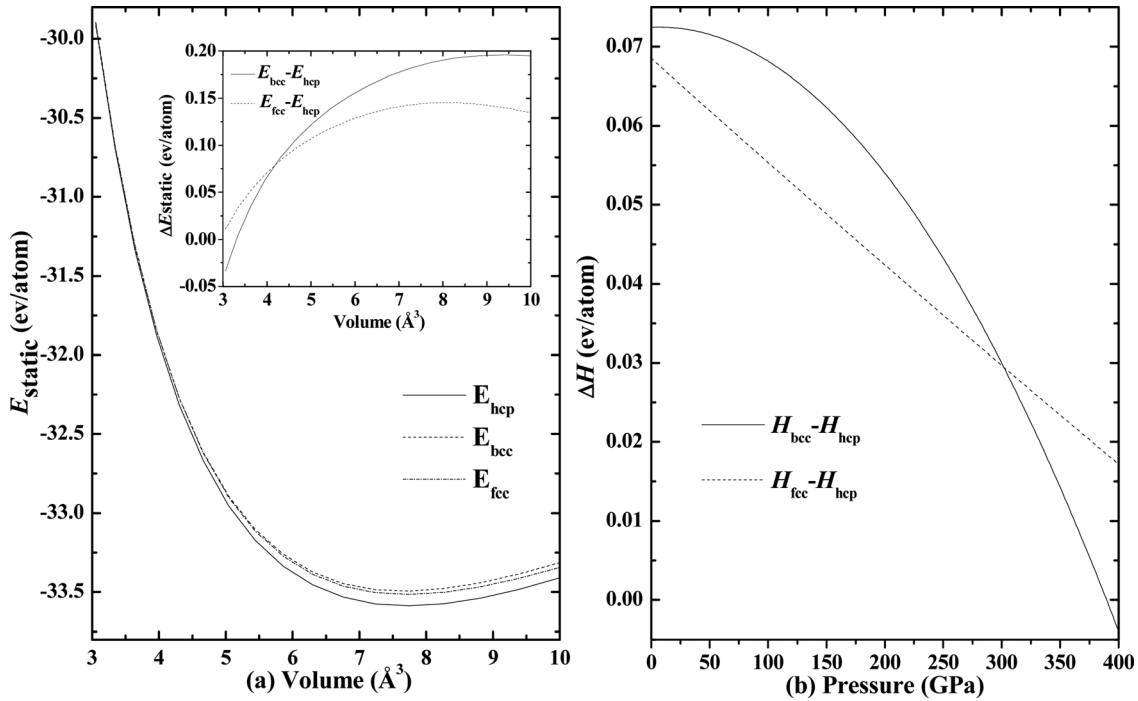


FIG. 1. (a) Static energy per atom of the bcc, fcc, and hcp phases as function of volume. (b) Enthalpy per atom of the bcc and fcc phases relative to the bcc enthalpy as function of pressure.

$$C_{33} - P = \rho_1 \left. \frac{d^2 E(\rho_1, \hat{\epsilon}_5)}{d\gamma^2} \right|_{\gamma=0}. \quad (10)$$

III. RESULTS AND DISCUSSION

A. Structural and elastic properties

We calculated the static energy-volume (E - V) curves for hcp, bcc, and fcc structures. Figure 1(a) shows the static energy of the hcp, bcc, and fcc as a function of volume. The static energy differences are plotted in the inset of Fig. 1(a). For the applied wide range of volume, the static energy difference between fcc and hcp is positive. By fitting the E - V data to the fourth-order finite strain EOS,³³ we calculated the enthalpy versus pressure for the three structures at zero temperature [Fig. 1(b)]. The transformation from hcp to bcc occurs at 390 GPa, in good agreement with experiments,^{6–8} and theoretical calculations.^{13,14} Therefore, in the present work, all calculations were performed for the hcp phase. The equilibrium volume V_0 , lattice parameters a and c , the bulk modulus B_0 , and its pressure derivative B' , are list in Table I. Our results are also in excellent agreement with the available experimental data.^{34–37} We note that the bulk modulus of hcp Be at 0 K is 122 GPa, and decreases to 118 GPa when thermal effects are included.

The elastic constants of hcp Be at each volume were calculated using the method discussed above. The pressure was obtained from the static equation of state. Table II summaries the calculated elastic constants at equilibrium structure parameters, together with the experimental data¹⁵ and previous calculations.^{12,20} Our results agree well with both sets of data. From Table II, one can see that all the elastic constants are practically linear increasing as pressure increases. Consequently, we fit the calculated elastic constants as the form

$C_{ij}(P) = a_{ij} + b_{ij}P$, and tabulated the fitting parameters in Table III. Recently, Cazorla *et al.*³⁸ have found similar trends in hcp He using atomistic Diffusion Monte Carlo calculations that fully account for ionic quantum effects. The errors of all elastic constants are $\sim 4\%$ in our results, which due to the uncertainties of the energies and corresponding polynomial fits. For a stable hexagonal structure, its five independent elastic constants C_{ij} should satisfy the mechanical stability criteria, i.e., $\tilde{C}_{44} > 0$, $\tilde{C}_{11} > |\tilde{C}_{12}|$, and $\tilde{C}_{33}(\tilde{C}_{11} + \tilde{C}_{12}) > 2\tilde{C}_{13}^2$, where $\tilde{C}_{\alpha\alpha} = C_{\alpha\alpha} - P$ ($\alpha = 1, 3, 4$), $\tilde{C}_{12} = C_{12} + P$, $\tilde{C}_{13} = C_{13} + P$. Clearly, these calculated elastic constants C_{ij} satisfy the mechanical stability criteria, suggesting that hcp Be is mechanically stable under the applied pressure.

Based on the Voigt-Reuss-Hill approximation,³⁹ we have calculated the corresponding bulk, shear and Young's modulus from the single crystal elastic constants. Then the isotropic averaged aggregate velocities can be obtained as follows

$$V_P = [(B + 4/3G)/\rho]^{1/2}, \quad (11)$$

$$V_B = (B/\rho)^{1/2}, \quad (12)$$

TABLE I. The equilibrium volume V_0 ($\text{\AA}^3/\text{atom}$), lattice parameters a and c , axial ratio c/a , zero pressure bulk modulus B_0 (GPa), and pressure derivative B' .

		V_0	a	c	c/a	B_0	B'
hcp	present	7.723	2.248	3.529	1.57	122	3.29
	Present*	7.910	2.266	3.556	1.569	118	3.21
	experimental	8.105 ³⁴	2.285 ³⁴	3.585 ³⁴	1.569 ³⁴	118 ³⁶	3.52 ³⁶
	experimental	8.110 ³⁵	2.286 ³⁵	3.584 ³⁵	1.568 ³⁵	119 ³⁷	3.48 ³⁷
bcc	Present	7.665	2.484			120	3.34
fcc	Present	7.710	3.136			118	3.33

The asterisk * indicates the values obtained from 300 K EOS.

TABLE II. The calculated elastic constants and anisotropies Δ_p , Δ_{S1} , and Δ_{S2} for the three types of elastic waves of hcp Be, compared with the experimental data and the other theoretical results. C_{ij} , B , G , and E are in GPa.

P	C_{11}	C_{12}	C_{13}	C_{33}	C_{44}	B	G	E	Δ_p	Δ_{S1}	Δ_{S2}
0	310.9	19.5	19.1	359.5	162.1	121.6	155.3	326.7	1.156	0.975	1.113
25.11	487.03	34.95	26.13	553.56	233.42	188.9	234.3	497.3	1.137	1.059	1.033
50.02	643.8	50.37	32.45	724.04	296	248.9	303.7	647.8	1.125	1.100	0.998
75.04	792.43	65.48	39.31	890.23	353.07	306.8	368.6	789.6	1.123	1.136	0.971
100.03	935.27	80.78	46.54	1049.29	407.74	362.8	430.6	925.7	1.122	1.160	0.954
125.01	1072.31	97.62	54.09	1192.8	460.04	416.4	489	1054.3	1.112	1.172	0.944
150.15	1210.32	111.35	61.49	1353.04	511.17	471.1	548.7	1185.7	1.118	1.194	0.930
174.88	1342.38	127.04	68.99	1498.32	560.18	523.4	604.8	1309.9	1.116	1.206	0.922
200.41	1477.5	142.98	76.33	1643.9	609.61	576.4	661.8	1435.9	1.113	1.217	0.914
224.98	1606.3	158.8	84.75	1782.61	656.06	627.7	715.5	1555.6	1.110	1.227	0.906
249.98	1734.35	174.72	92.89	1935.06	702.45	680.2	769.9	1677	1.116	1.240	0.901
274.88	1861.42	190.7	101.58	2055.69	748.12	729.4	821.8	1792.3	1.104	1.241	0.896
299.9	1988.74	207.08	109.57	2215.09	791.86	782.5	875.1	1912.4	1.114	1.258	0.889
Exp. (Ref. 15)	293.6	26.8	14	356.7	162.2	116.8	150.1	315.2	1.215	0.959	1.216
Ref. 12	300.8	14.1	7.1	359.5	160.2	112.8	154.5	318.2	1.195	1.008	1.118
Ref. 20	305.9	18.8	10.4	329	159.3	114.5	152.4	316.7	1.076	0.964	1.110

$$V_S = (G/\rho)^{1/2}, \quad (13)$$

where V_P , V_B , and V_S are the compressional, bulk, and shear sound velocities, respectively. In addition, as listed in Table II, the bulk modulus B deduced from elastic constants turns out to be very close to that obtained by EOS fitting. This indicates that our calculations are consistent and reliable. The bulk modulus, shear modulus, Young's modulus, and all the sound velocities increase monotonously with pressure increasing, as presented in Figs. 2(a) and 2(b).

It is known that the acoustic velocities are related to the elastic constants by the Christoffel equation⁴⁰

$$(C_{ijkl}n_jn_k - M\delta_{il})u_i = 0, \quad (14)$$

where C_{ijkl} is the fourth-rank tensor description of the elastic constants, n is the propagation direction, ρ is the density, and u is the polarization vector. The acoustic anisotropy can be described as⁴¹

$$\Delta_i = \frac{M_i[n_x]}{M_i[100]}, \quad (15)$$

where n_x is the extremal propagation direction, and i denotes the three types of elastic waves (one longitudinal and two polarizations of the shear wave). By solving the Christoffel equation for hcp Be, one can obtain the anisotropy of the compressional wave (P), $\Delta_p = C_{33}/C_{11}$, and the anisotropies of the wave polarized perpendicular to the basal plane ($S1$) and the polarized one in the basal plane ($S2$), $\Delta_{S1} = (C_{11} + C_{33} - 2C_{13})/4C_{44}$, $\Delta_{S2} = 2C_{44}/(C_{11} - C_{12})$.

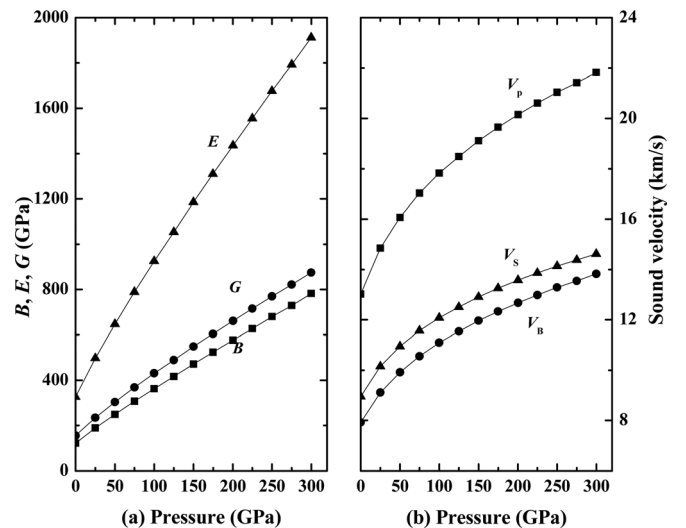
TABLE III. Value of the parameters obtained in the linear fits to our $C_{ij}(P)$ results. a_{ij} is given in units of GPa, and b_{ij} is given in GPa/K.

	C_{11}	C_{12}	C_{13}	c_{33}	C_{44}
a_{ij}	327.89	19.43	18.58	378.72	173.15
b_{ij}	5.78	0.61	0.29	6.36	2.18

The calculated pressure dependences of the anisotropies Δ_p , Δ_{S1} and Δ_{S2} for the three types of elastic waves are illustrated in Table II. It is noted that with Δ_{S2} and Δ_p decrease as pressure increases, while Δ_{S1} increases with the pressure increasing. We also noted that as the pressure increases the values of Δ_{S1} and Δ_{S2} goes away from 1.0, which indicates that the anisotropies of the wave polarized perpendicular to the basal plane ($S1$) and the wave polarized in the basal plane ($S2$) become strong.

B. Phonon dispersions and phase transition

Within the DFPT, we obtained phonon dispersion curves of hcp and bcc Be along high-symmetry directions. In Fig. 3(a), we compare our results with the experimental dispersion curves¹⁹ at 80 K. The agreement between the two sets of data is impressive, and typical of DFPT. The hcp phase of Be is dynamically stable at zero pressure as the phonon

FIG. 2. (a) Bulk modulus B , shear modulus G , and Young's modulus E vs pressure at zero temperature. (b) Aggregate sound velocities (V_P , V_B , and V_S) vs pressure at zero temperature.

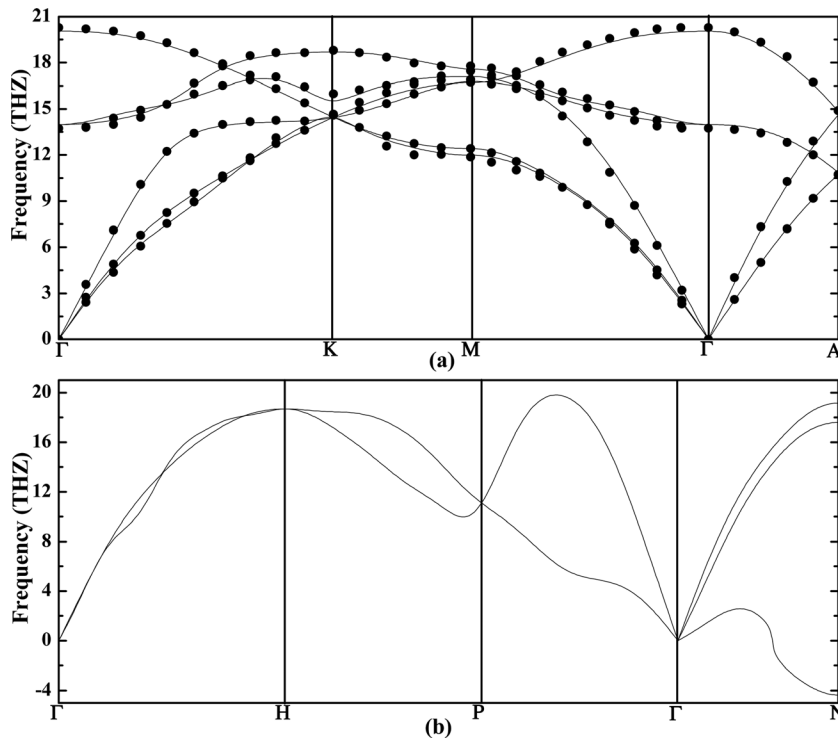


FIG. 3. Phonon dispersion curves of (a) hcp Be, (b) bcc Be at 0 GPa and 0 K. The solid circles in (a) are neutron diffraction data (Ref. 19) measured at 80 K.

frequencies do not show any anomaly. The calculated phonon dispersions for bcc Be are displayed in Fig. 3(b). Note that the frequencies around N point along $\Gamma-N$ in the transverse acoustical branch soften to imaginary frequencies, indicating dynamic instability.

To understand the dynamic stability of hcp and bcc Be at high pressure, it is useful to investigate lattice vibrations at different volumes. Figure 4(a) shows that the frequencies in the dispersion curves of hcp Be increase with decreasing volume. We do not find soft modes in the applied range of volumes, and the phonon frequencies reflect the dynamic stability. The calculated phonon dispersions at different volumes for bcc Be are displayed in Fig. 4(b), also for bcc, our results show that the phonon frequencies increase as volume decreases. The calculations predict the stability of the bcc phase of Be, and the frequencies of the phonons along the $\Gamma-N$ symmetry line and around the N symmetry point are real.

In order to obtain accurately Helmholtz free energy F as functions of volume V at a certain temperature, the F at 17 atomic volumes (between $V=3$ and $8 \text{ \AA}^3/\text{atom}$) for hcp and bcc phases have been calculated. We determined the phase transition pressure by comparing the Gibbs free energies of hcp and bcc Be. The Gibbs free energy G is calculated from the Helmholtz free energy as $G(P,T) = F(V,T) + PV$. Within QHA, the transition pressure is calculated at various temperatures up to 3500 K. The phase diagram of Be at high pressure and temperature is shown in Fig. 5, compared with theoretical calculation.²¹ It can be seen that the phase transition from hcp to bcc at 386 GPa at 300 K, which indicates that at ambient temperature the hcp phase is more stable than the bcc phase. Most experiments⁶⁻⁸ have not detected any kind of phase transition up to 300 GPa. Robert *et al.*^{14,21} found that the hcp Be is the most stable phase up to 400 GPa. In Fig. 5, the dotted line is from the calculations of

Robert *et al.*,²¹ who obtained the phase diagram with the QHA. Our transition pressures are consistent with those calculated by Robert *et al.*²¹ at low temperatures, and show a small deviation at high temperatures, which mainly due to the choice of the LDA functional.

C. Thermodynamic properties

The Helmholtz free energy and phonon contribution F_{phon} as functions of volume V and temperature T can be derived from Eq. (1) and (2), respectively. The thermal free energy arising from electronic excitations F_{elec} and the phonon contribution F_{phon} as functions of volume at temperatures from 300 to 3500 K are shown in Figs. 6(a) and 6(b). By fitting the Helmholtz free energy to the fourth-order finite strain EOS at each temperature, we get the theoretical isothermal compressional curves, as shown in Fig. 7. We estimate the errors of the Helmholtz free energy are less than 0.02%, which derived from the uncertainties of the energies and corresponding EOS fits. Including the zero point energy (ZPE) to the free energy at 0 K raises the equilibrium volume by 1.9% and reduces the bulk modulus by 2 GPa relative to the values without ZPE. It is noted that the 0 K isotherm (including ZPE) is almost the same as the 300 K one, and this is due to the small free energy contribution from the lattice vibrations at 300 K. With the pressure increasing, our isotherms agree with the experimental data.⁸

The thermal pressure can be obtained from the pressure difference with the 0 K isotherm. The thermal pressure as functions of volume and temperature are shown in Figs. 8(a) and 8(b). From Fig. 8(a), one notes that the thermal pressures show little volume dependence at low temperature. At elevated temperature, the thermal pressure increases significantly, and decreases monotonously with increasing volume.

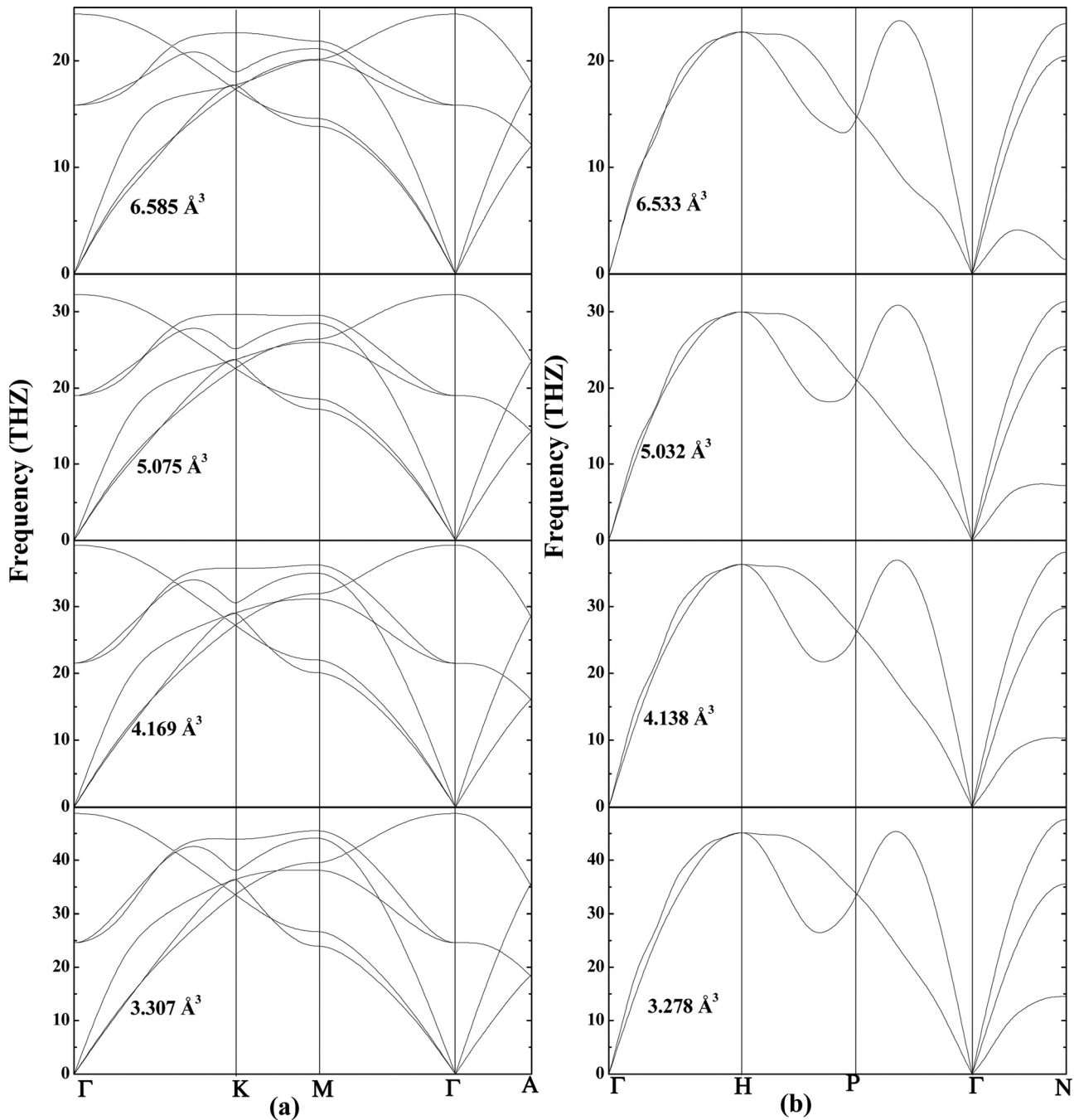


FIG. 4. The phonon dispersion curves of the hcp (a) and bcc (b) Be shown along high-symmetry directions at different volumes.

The thermal pressures as a function of temperature are shown in Fig. 8(b). At a given volume, the thermal pressure increases linearly with temperature. The slopes of the thermal pressure show strong volume dependence. Many previous calculations for metals (such as Mo³⁰ and Ta⁴² and so on) also found that the slopes of the thermal pressure were strongly volume dependent.

To check the accuracy of our thermal EOS at high pressures, we calculated the Hugoniot P - V and P - T curves by solving the Rankine-Hugoniot equation:

$$U_H - U_0 = \frac{1}{2}(P_H + P_0)(V_0 - V_H), \quad (16)$$

where U_H , P_H , and V_H are the molar internal energy, pressure, and volume along the Hugoniot states, respectively, and U_0 and V_0 are the molar internal energy and volume at zero pressure P_0 and room temperature. For a given volume, we adjusted temperature and obtained pressure and energy until the Rankine-Hugoniot relation was satisfied. We obtained the pressure–volume and temperature–pressure relations along the Hugoniot curve according to Eq. (16). Figure 9 shows the obtained Hugoniot curve of P - V and P - T . Our obtained Hugoniot curves are in excellent agreement with experiments⁴³ and other calculations.^{14,44,45} Our P - T curve agrees well with the theoretical predictions of Robert *et al.*¹⁴ and Holian *et al.*,⁴⁴ and deviated from Song *et al.*⁴⁵

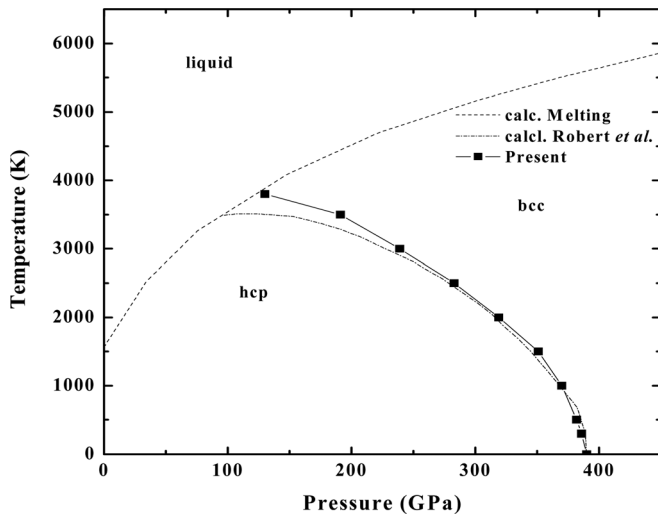


FIG. 5. Phase diagram of Be at high pressure and temperature. The dotted line is the hcp-bcc boundary calculated by Robert *et al.* (Ref. 21), the dashed line is the theoretical melting curve by Robert *et al.* (Ref. 21).

The thermal expansion coefficient α_V is defined as:

$$\alpha_V = \frac{1}{V} \left(\frac{\partial V}{\partial T} \right)_P. \quad (17)$$

The thermal expansion coefficient as functions of pressure and temperature are plotted in Figs. 10(a) and 10(b). In Fig. 10(a), it is showed that our zero pressure results are in excellent agreement with the experimental data⁴⁶ at high temperature. The discrepancy between the calculated thermal expansion coefficients and the experimental results at high temperature might be attributed to the use of the LDA func-

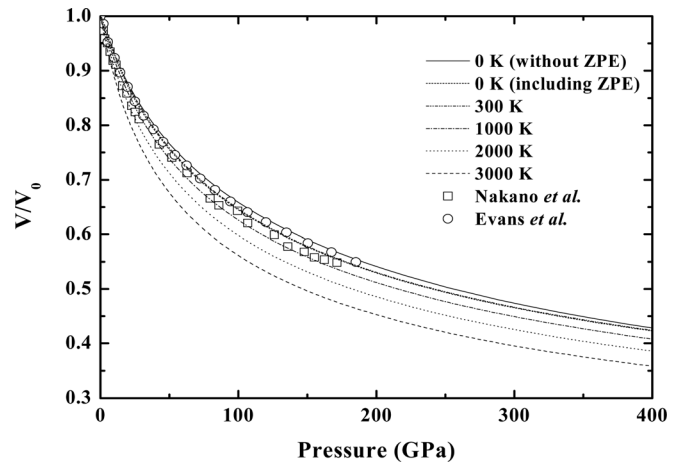


FIG. 7. Isothermal compression curves at different temperatures, compared with experimental data (Refs. 6, 8).

tion. At ambient conditions, our calculated thermal expansion coefficient is $3.43 \times 10^{-5} \text{ K}^{-1}$, consistent with the experimental value $3.4 \times 10^{-5} \text{ K}^{-1}$.⁴⁷ As the pressure rises, the thermal expansion coefficient increases with temperature, and then converges to a nearly constant value at high temperature. The thermal expansion coefficient decreases strongly with increasing pressure in Fig. 10(b).

The specific heat at constant volume is defined by

$$C_V = \left(\frac{\partial U}{\partial T} \right)_V, \quad (18)$$

where U is the internal energy of the system. The specific heat at constant pressure C_P is different from C_V due to the

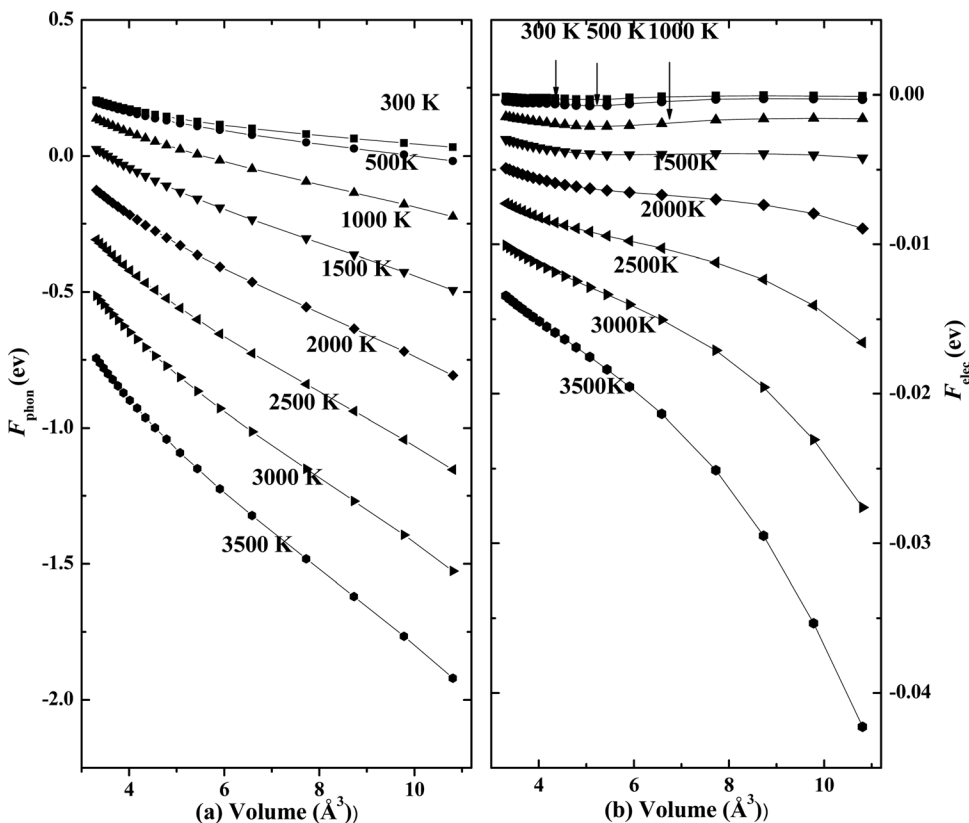


FIG. 6. Free energy from the phonons F_{phon} (a) and electronic excitations F_{elec} (b) vs volume of hcp Be at temperatures from 300 to 3500 K.

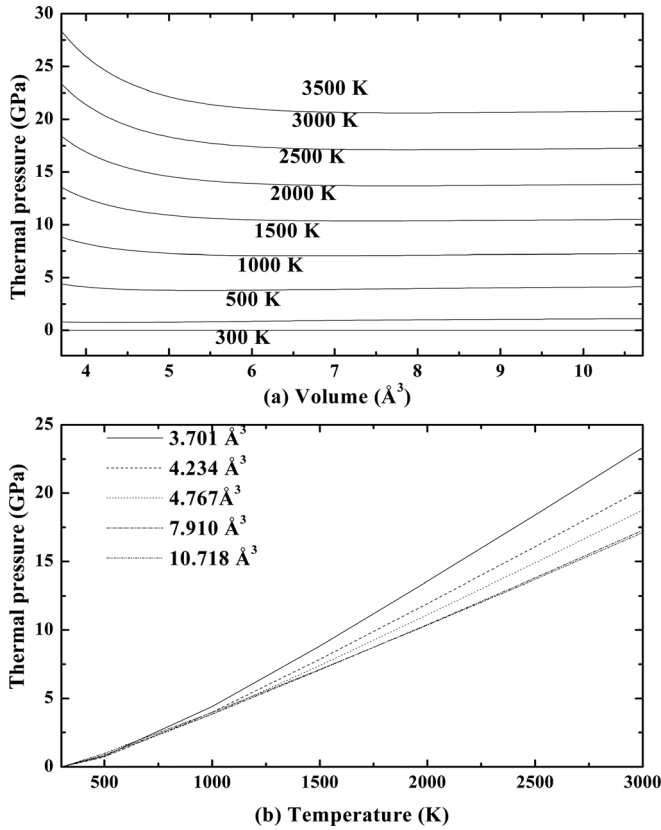


FIG. 8. Calculated thermal pressures of hcp Be (a) as a function of volume and (b) temperature.

thermal expansion caused by anharmonic effects. The relationship between C_P and C_V is given by

$$C_P - C_V = \alpha_V^2(T)B_0VT, \quad (19)$$

where α_V is the volume thermal expansion coefficient, and B_0 the bulk modulus. In a harmonic crystal C_V increases at low temperature and approaches the constant $3R$ at high temperature. In Fig. 11, we plot C_P , which decreases with pressure, and increases with temperature. The available experimental results⁴⁸ at zero pressure are also plotted as squares for comparison. It is evident that our QHA results are in overall good agreement with the experimental data at zero pressure, but diverge at high temperature. It is found that C_P is obvious different between low and high pressures with increasing temperature beyond 1600 K (about the melting temperature), which implies that validity of QHA cannot be extended to high temperature at low pressure and we should consider higher-order anharmonicities. The melting temperature increases with pressure, and since the QHA is only valid up to some fraction of the melting temperature, then the validity of the QHA extends to higher temperatures at higher pressures.

The thermodynamic Grüneisen parameter is a very important parameter through which the thermal pressure is related to the increase of thermal energy in the Mie–Grüneisen equation of state and it is defined by

$$\gamma = V \left(\frac{\partial P}{\partial U} \right)_V = \frac{\alpha_K T V}{C_V}, \quad (20)$$

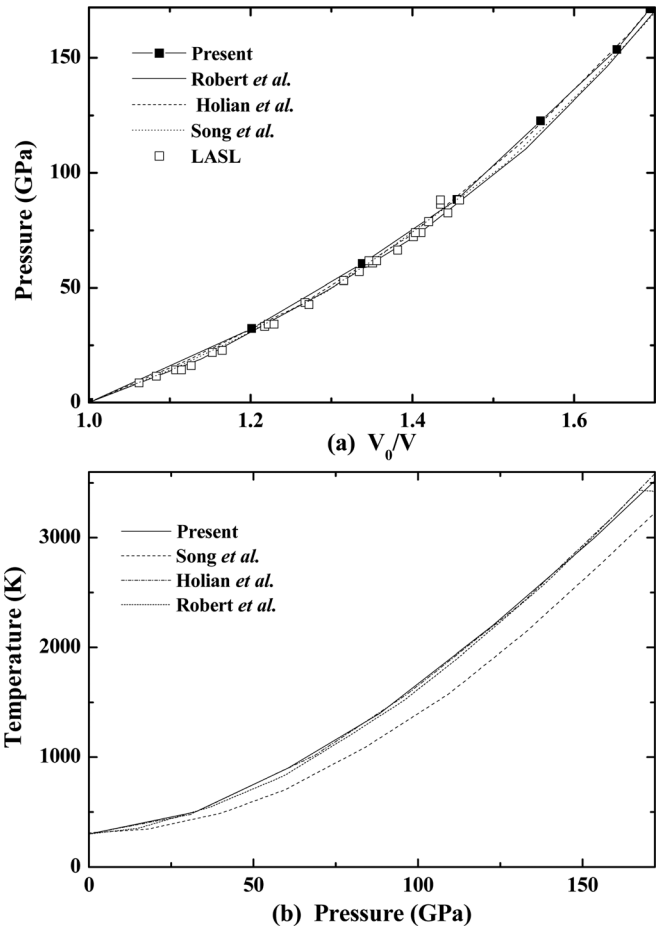


FIG. 9. Volume–pressure (a) and temperature–pressure (b) relations on Hugoniot curves obtained from the QHA, in comparison with experimental data (Ref. 43) and other calculations (Refs. 14, 44, 45).

where U is the internal energy of the system. Our calculated zero-pressure 300 K value of γ is 1.271, very close the experiment value 1.203.¹⁵ The value of γ versus temperature and pressure are shown in Figs. 12(a) and 12(b), respectively. From Fig. 12(a), it is obvious that γ shows weak dependence on temperature along the isobar. Upon compression, γ decreases significantly, but the temperature effects become less pronounced [Fig. 12(b)]. In addition, the values of γ at high pressures remain nearly constant.

Within the Debye approximation, the Helmholtz free energy at low temperature is

$$F = E_{static} + RT \left[\frac{9}{8} \left(\frac{\Theta_D}{T} \right) + 3 \ln(1 - e^{-\Theta_D/T}) - D \left[\frac{\Theta_D}{T} \right] \right], \quad (21)$$

$D(\Theta_D/T)$ is the Debye function written as

$$D(\Theta_D/T) = 3 \left(\frac{T}{\Theta_D} \right)^3 \int_0^{\Theta_D/T} \frac{z^3 dz}{e^z - 1}. \quad (22)$$

We obtained Θ_D at temperature T by solving Eq. (21). Our results for the Debye temperature are displayed in Fig. 13. Θ_D shows a significant increase as pressure increases (decrease of volume). At fixed volume, Θ_D drops with increasing T up to ~ 100 K, and then decreases moderately in the temperature

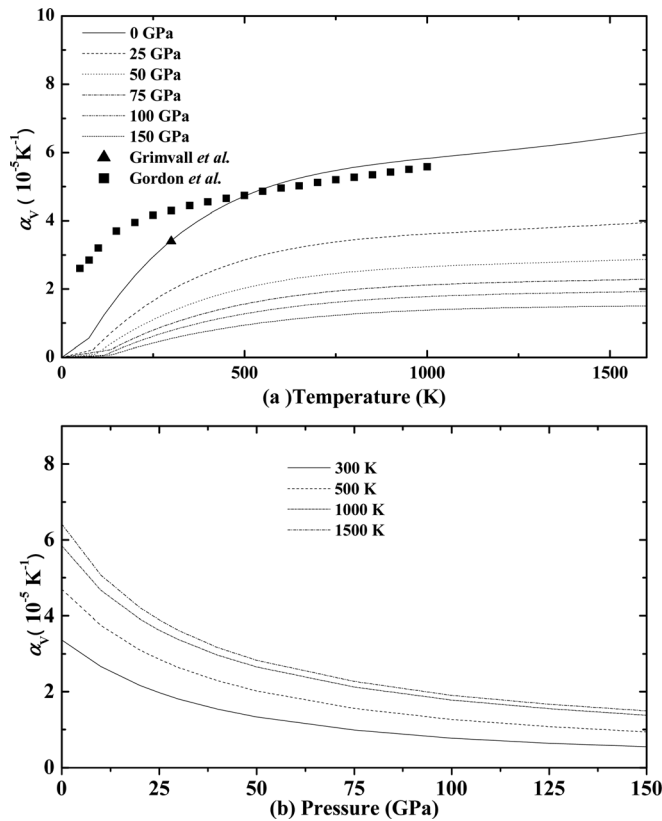


FIG. 10. Thermal expansion coefficient α_V as a function of temperature (a) and pressure (b). The solid squares and solid triangle are taken from Gordon *et al.* (Ref. 46) and Grimvall *et al.* (Ref. 47), respectively.

range from around 100 to 300 K. With further increase of T (above 300 K), Θ_D shows weak temperature dependence, especially at high pressure. At 300 K and 0 GPa, the obtained value of Θ_D is 930 K, which is consistent with the experimental values of 949 ± 51 K.⁴⁹⁻⁵¹

IV. CONCLUSIONS

We employed the density functional perturbation theory to investigate the phase transition, elastic properties, lattice

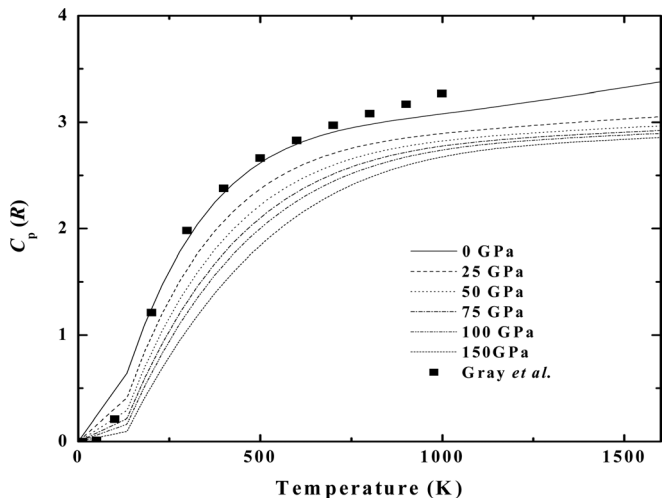


FIG. 11. Heat capacity C_p as a function of temperature at different pressure, together with the experimental data (Ref. 48).

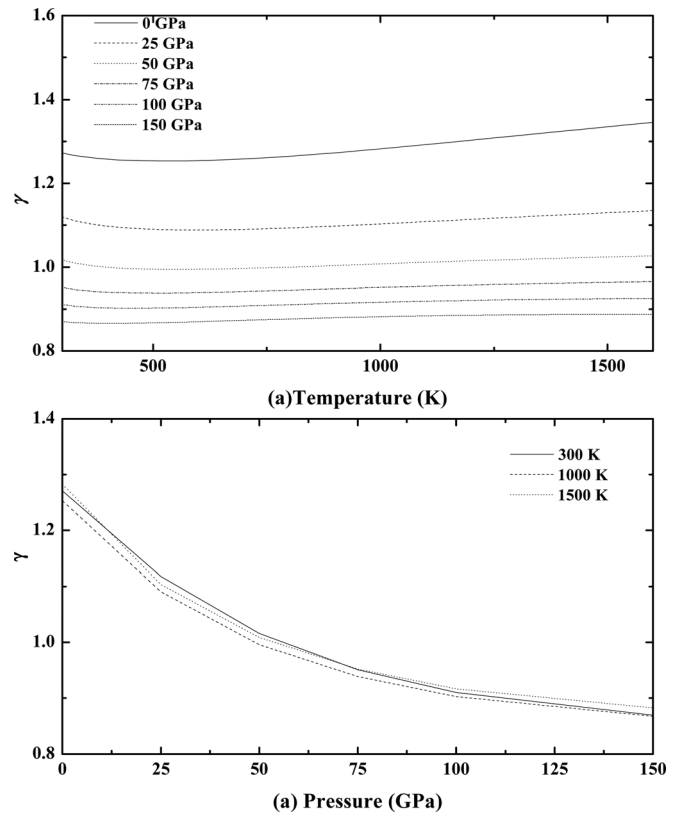


FIG. 12. Variation of the Grüneisen parameter γ with temperature (a) and pressure (b).

dynamical properties, and thermodynamic properties of the hcp structure of Be. By comparing the static energy-volume and enthalpy-pressure curves for the hcp, bcc, and fcc Be, we found that the stable phase of Be is hcp at zero pressure and temperature and then transforms to bcc Be at 390 GPa. The fcc phase is never be the stable phase in the whole range of pressures. At ambient conditions, the calculated elastic constants agree well with the experimental data. From the elastic constants at high pressure, we found that hcp Be is stable. Bulk, shear, and Young's modulus, and all the sound velocities as a function of pressure are obtained.

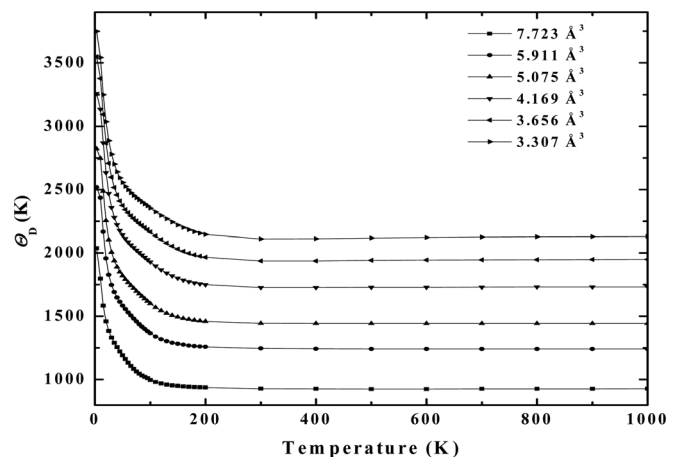


FIG. 13. Debye temperature Θ_D as a function of temperature at different volumes.

Our calculated phonon dispersion curve of hcp Be at zero GPa agree extremely well with experiment. Under compression, the dispersion curves of hcp Be do not show any anomaly or instability. The frequencies of bcc Be along Γ - N in the T_1 branches soften to imaginary frequencies at zero pressure, indicating a structural instability, while with pressure increasing, the imaginary frequencies of bcc Be along Γ - N in the T_1 branches shift to positive frequencies. With the QHA, the hcp-bcc boundary under high temperature and pressure was obtained. Our results agree well with those reported by Robert *et al.* We predicted the thermal EOS properties including thermal EOS, thermal pressure, volume thermal expansion, and Hugoniot properties. The zero-pressure-temperature dependencies of volume thermal expansion coefficient, Grüneisen parameter, and Debye temperature are found to be in a good agreement with the experimental results. The QHA is only valid up to a fraction of the melting temperature, and therefore results can only be expected to agree with experiments at sufficiently low temperatures. Since the melting temperature increases with pressure, the validity of the results extends to higher temperatures with increasing pressure.

ACKNOWLEDGMENTS

The authors would like to thank Dr. Zhao-Yi Zeng for the helpful discussions. We also thank the support by the National Natural Science Foundation of China under Grant Nos. 10776029/A06 and 11174214, the Specialized Research Fund for the Doctoral Program of Higher Education under Grant No. 20090181110080 and the Science Foundation of China Academy of Engineering Physics under Grant No. 2010A0101001.

- ¹K. L. Wilson, R. A. Causey, W. L. Hsu, B. E. Mills, M. F. Smith, and J. B. Whitley, *J. Vac. Sci. Technol. A* **8**, 1750 (1990).
- ²K. Kádás, L. Vitos, B. Johansson, and J. Kollár, *Phys. Rev. B* **75**, 035132 (2007).
- ³D. A. Young, *Phase Diagrams of the Elements* (University of California Press, Berkeley, CA, 1991).
- ⁴J. Elmsley, *The Elements* (Oxford University Press, London, 1998).
- ⁵L. C. Ming and M. H. Manghnani, *J. Phys. F: Met. Phys.* **14**, L1 (1984).
- ⁶K. Nakano, Y. Akahama, and H. Kawamura, *J. Phys.: Condens. Matter* **14**, 10569 (2002).
- ⁷N. Velisavljevic, G. N. Chestnut, Y. K. Vohra, S. T. Weir, V. Malba, and J. Akella, *Phys. Rev. B* **65**, 172107 (2002).
- ⁸W. J. Evans, M. J. Lipp, H. Cynn, C. S. Yoo, M. Somayazulu, D. Häusermann, G. Shen, and V. Prakapenka, *Phys. Rev. B* **72**, 094113 (2005).
- ⁹P. K. Lam, M. Y. Chou, and M. L. Cohen, *J. Phys. C* **17**, 2065 (1984).
- ¹⁰J. Meyer-ter-Vehn and W. Zittel, *Phys. Rev. B* **37**, 8674 (1988).
- ¹¹B. Palanivel, R. S. Rao, B. K. Godwal, and S. K. Sikka, *J. Phys.: Condens. Matter* **12**, 8831 (2000).
- ¹²G. V. Sin'ko and N. A. Smirnov, *Phys. Rev. B* **71**, 214108 (2005).
- ¹³L. X. Benedict, T. Ogitsu, A. Trave, C. J. Wu, P. A. Sterne, and E. Schwegler, *Phys. Rev. B* **79**, 064106 (2009).
- ¹⁴G. Robert, A. Sollier, and Ph. Legend, in *Shock Compression of Condensed Matter—2007*, edited by Mark Elert, Michael D. Furnish, Ricky Chau, Neil Holmes, and Jeffrey Nguyen, AIP Conf. Proc. No. 955 (AIP, New York, 2007), p. 97.
- ¹⁵A. Migliori, H. Ledbetter, D. J. Thoma, and T. W. Darling, *J. Appl. Phys.* **95**, 2436 (2004).
- ¹⁶W. D. Rowland and J. S. White, *J. Phys. F: Met. Phys.* **2**, 231 (1972).
- ¹⁷Y. I. Kokovikhin, *Strength Mater.* **22**, 1616 (1990).
- ¹⁸K. Kádás, L. Vitos, R. Ahuja, B. Johansson, and J. Kollár, *Phys. Rev. B* **76**, 235109 (2007).
- ¹⁹R. Stedman, Z. Amilius, R. Pauli, and O. Sundin, *J. Phys. F: Met. Phys.* **6**, 157 (1976).
- ²⁰G. Robert and A. Sollier, *J. Phys. IV* **134**, 257 (2006).
- ²¹G. Robert, P. Legend and S. Bernard, *Phys. Rev. B* **82**, 104118 (2010).
- ²²S. Baroni, P. Giannozzi, and A. Testa, *Phys. Rev. Lett.* **58**, 1861 (1987).
- ²³S. Baroni, S. D. Gironcoli, A. D. Corso, and P. Giannozzi, *Rev. Mod. Phys.* **73**, 515 (2001).
- ²⁴S. Baroni, A. D. Corso, S. de Gironcoli, P. Giannozzi, C. Cavazzoni, G. Ballabio, S. Scandolo, G. Chiarotti, P. Focher, A. Pasquarello, K. Laasonen, A. Trave, R. Car, N. Marzari, and A. Kokalj, see <http://www.pwscf.org/> for more information about the quantum-simulation software.
- ²⁵W. Kohn and L. J. Sham, *Phys. Rev. B* **140**, A1133 (1965).
- ²⁶J. P. Perdew and A. Zunger, *Phys. Rev. B* **23**, 5048 (1981).
- ²⁷B. Hammer, L.B. Hansen, and J.K. Norskov, *Phys. Rev. B* **59**, 7413 (1999).
- ²⁸H. J. Monkhorst and J. D. Pack, *Phys. Rev. B* **13**, 5188 (1976).
- ²⁹L. Fast, J. M. Wills, B. Johansson, and O. Eriksson, *Phys. Rev. B* **51**, 17431 (1995).
- ³⁰Z. Y. Zeng, C. E. Hu, L. C. Cai, X. R. Chen, and F. Q. Jing, *J. Phys. Chem. B* **114**, 298 (2010).
- ³¹C. E. Hu, Z. Y. Zeng, L. Zhang, X. R. Chen, L. C. Cai, and D. Alfè, *J. Appl. Phys.* **107**, 093509 (2010).
- ³²G. V. Sin'ko and N. A. Smirnov, *J. Phys.: Condens. Matter* **14**, 6989 (2002).
- ³³F. Birch, *J. Geophys. Res.* **91**, 4949 (1986).
- ³⁴V. M. Amonenko, V. Ye. Ivanov, G. F. Tikhinskij, and V. A. Finkel, *Phys. Met. Metallogr.* **14**, 47 (1962).
- ³⁵K. J. H. Mackay and N. A. Hill, *J. Nucl. Mater.* **8**, 263 (1963).
- ³⁶J. L. Wise, L. C. Chhabildas, and J. R. Asay, in *Shock Waves in Condensed Matter-1981*, AIP Conf. Proc. No.78, edited by W. J. Nellis, L. Seaman, and R. A. Graham (AIP, New York, 1982), p. 417.
- ³⁷T. Neal, in *High Pressure Science and Technology*, edited by K. D. Timmerhaus and M. S. Barber (Plenum, New York, 1974), pp. 1 and 80.
- ³⁸C. Cazorla, Y. Lutsyshyn and J. Boronat, *Phys. Rev. B* **85**, 024101 (2012).
- ³⁹R. Hill, *Proc. Phys. Soc. London* **65**, 350 (1952).
- ⁴⁰P. Ravindran, P. Vajeeston, R. Vidya, A. Kjekshus, and H. Fjellvåg, *Phys. Rev. B* **64**, 224509 (2001).
- ⁴¹G. Steinle-Neumann, L. Stixrude, and R. E. Cohen, *Phys. Rev. B* **60**, 791 (1999).
- ⁴²S. Taioli, C. Cazorla, M. J. Gillan, and D. Alfè, *Phys. Rev. B* **75**, 214103 (2007).
- ⁴³*LASL Shock Hugoniot Data*, edited by S. P. Marsh (University of California Press, Berkeley, 1980).
- ⁴⁴K.S. Holian, Los Alamos National Laboratory Report LA-10160-MS UC-34 (1984).
- ⁴⁵H. F. Song and H. F. Liu, *Phys. Rev. B* **75**, 245126 (2007).
- ⁴⁶P. Gordon, *J. Appl. Phys.* **20**, 908 (1949).
- ⁴⁷G. Grimvall, *Thermophysical Properties of Materials* (Elsevier Science B. V., Netherlands, 1999), p. 214.
- ⁴⁸D. E. Gray, *American Institute of Physics Handbook* (McGraw-Hill, New York, 1972).
- ⁴⁹O. Hunderi and H. P. Myers, *J. Phys. F: Met. Phys.* **4**, 1088 (1974).
- ⁵⁰C. A. Swenson, *J. Appl. Phys.* **70**, 3046 (1991).
- ⁵¹N. Gopi Krishna and D. B. Sirdeshmukh, *Acta Crystallogr. A* **54**, 513 (1998).